



Experimental Investigation of Nickel Ferrite (NiFe₂O₄)-Based Nano-magnetorheological Fluid Characteristics Using MR Damper Under Triangular Displacement Excitation

Padma Yagnasri¹ · Nuthalapati Seetharamaiah² · Usha Sri Pantangi¹

Received: 24 September 2021 / Revised: 6 April 2022 / Accepted: 11 April 2022 / Published online: 29 April 2022
© Krishtel eMaging Solutions Private Limited 2022

Abstract

The fluid characteristics of the MR damper have a notable impact on its design and overall conduct of the damper application devices. First, the hydraulic circuit design features of the MR damper are introduced and then the detailed testing scheme of the damper was proposed. The damping characteristics of fluid were tested under the triangular displacement excitation to study the performance and know the accurate amount of damping force. The test data were recorded at various piston velocities (V_p) maintaining constant damper coil input current. The input current will produce the magnetic field and influence the nano-magnetorheological fluid (NMRF) flow across the gaps to achieve maximum damping performance. The experimental outcomes show that the fluid in MR damper has a typical feature of linearity and symmetry. The theoretical data were calculated using quasi-static model to validate the efficacy of the experimental data. The theoretical results are in good agreement with the experimental data.

Keywords Fluid characteristics · Input current · MR damper · Nano-magnetorheological fluid · Piston velocity · Triangular displacement excitation

Introduction

Magnetorheological fluid devices developed have advanced for materialistic production because of their innovations in material sciences. These devices are categorized as fixed pole and movable pole devices, where magnetorheological dampers are an example for fixed pole devices [1]. The MR damper has the ability to alter its damping by shifting the magnetic field strength through the damper coil input current [2]. These dampers are characterized by high dynamic force range, very less power consumption, and short response time [3]. These advantages of MR dampers made its use in civil structures and earthquake-resistant structures [4].

In the recent years, MR dampers were used in different fields which include semi-active vibration control such as car, high speed train and seat suspension [5], cable bridges [6], aircraft landing gear [7], helicopter with multiple landing gears [8], seismic mitigation of building structures [9], washing machines [10], and prosthetic leg [11]. MR damper also have application in military combat and off road vehicles which require quick response and high damping forces with a heavy payload requirements [12]. The functionality of MR damper is comparable to conventional damper with little variances in structural features. The structural dampers are classified based on various modes. The dampers in flow or valve mode include linear damper [13]. Based on the structure the damper is classified into single-ended and double-ended piston rod type. The shear mode include rotary shock absorber [13] that was fitted on the vehicle chassis and was examined for the body resonance and comfort ride performance. The shear mode also includes linear shear mode, rotatory drum and rotatory disk damper [14]. The squeeze mode includes vibration dampers that are used in most of the industrial applications to control the damping forces [15]. The dampers in combination of flow and shear modes are classified in to single and double-ended piston

✉ Padma Yagnasri
yagnapadma1990@gmail.com

¹ Mechanical Engineering Department, University College of Engineering, Osmania University, Hyderabad, Telangana 500007, India

² Gitam University, Hyderabad campus, Rudraram, Patancheru mandal, Hyderabad, Telangana 502329, India

rod types [16]. The structure of a damper classified based on the combination modes is similar to the linear damper, the only difference is existence of annular circle gap with in the cylindrical case and piston.

Many researchers have proposed several models to assess the behavior of MR damper. Some of the models include dynamic models [17, 18], lumped mass model [19], multiphysics model [20], novel phenomenological model [21, 22], mathematical model for small MR damper [23], and its applications. Yao et al. [24] presented the MR damper application in semi-active vibration control of the vehicle suspension system. The Bouc–Wen model was adopted, with a specific semi-active control approach to assess the behavior of MR damper. The outcomes stated that with the consideration of semi-active control the vibration of the system was nicely managed. The simple analytical model comparative study was carried out to analyze the vibration reduction and the parameters that affect the enactment of damping [25]. Gordaninejad et al. [26] utilized the magnetorheological fluid damper along with steel and graphite epoxy concrete (G/E-C) supports to manage vibration of the scaled bridge and two span bridge. The results show the enhanced response of scaled model bridge along with G/E-C columns when compared to steel columns. But compared to passive MR damping control, the developed self-sensing MR damper that is developed based on linear quadratic Gaussian control (LQGC) achieves better control conduct and also effectively increases the damping force tracing [27]. Kim et al. [28] proposed the MR damper for aircraft landing gear to overcome the excitation and road conditions. The efficacy is presented in terms of field-dependent damping force and its improved efficiency. Aly [29] presented the dynamic building model for earthquake loads. A novel control algorithm was proposed to direct the MR damper. He reported that by placing the damper between the ground and first floor the seismic responses were reduced. Several other structural dynamic models were proposed for structural vibration mitigations [4, 30]. A novel self-adaptive MR damper [31], and a new sponge MR damper [32] was proposed to alleviate vibrations in a washing machines.

The analysis of damping force–velocity can be executed under different displacement excitations. Guan et al. [33] presented the dynamic enactment of the damper under sinusoidal displacement excitation. For the given displacement, the hysteresis width of the MR damper was a function of stiffness but independent of piston area on neglecting viscous element. The simulation and modeling of MR damper performance under triangular displacement excitation was investigated by Ramirez et al. [34].

In the present study, the following characteristics force–velocity, force–current, pressure–velocity and pressure–current effects were tested under the triangular displacement excitation to understand the essential conduct of

MR damper filled with the nano-magnetorheological fluid (NMRF). The test was conducted considering different velocities and constant damper coil input currents. The triangular excitation displacement amplitude of 12 mm was considered at different velocities 0, 0.05, 0.1, 0.15 and 0.2 m/s and damper coils input current were maintained constant at 0, 1, 2, 3 and 4 A. The experiments were conducted at room temperature (30 ± 1 °C) to reduce the temperature effects. The theoretical data were calculated using the quasi-static model [35].

Materials and Methods

The nickel ferrite (NiFe_2O_4) nanoparticles synthesized using sol gel technique [36] were used to prepare silicone oil and hydrocarbon oil-based NMRF samples. The particle size and concentration, and carrier oil are as shown in Table 1.

Experimental Testing of Fluid Damping Characteristics Under Triangular Displacement Excitation

In the present study, a small capacity prototype MR damper filled with NMRF was used and quasi-static experiments were conducted to test the damping characteristics of the fluid. The test system consists of hydraulic system, hydraulic cylinder, linear variable differential transformer (LVDT), data acquisition, load cell and so on. The experimental setup was constructed at Denison Hydraulics India Limited, Hyderabad. The schematic illustration and experimental testing setup is presented in Figs. 1 and 2. The small capacity MR damper is presented in Fig. 3 was used for testing the fluid characteristics. The scheme of experimental testing was designed as follows.

Hydraulic System

The actuator with a configuration of two no. 10 gpm Moog servo valves at a 60 Hz bandwidth drives the damper. The cylinder diameter of actuator is 50 mm and a stroke of 40 mm. To reduce the nonlinear effects, the actuator was equipped with less friction Teflon seals and it was managed

Table 1 NMRF components

Fluids	Particle size (nm)	Nanoparticle: carrier oil: surfactant volume concentration (%)
NMRF S	40–80	36:60:4
NMRF H	40–80	36:60:4

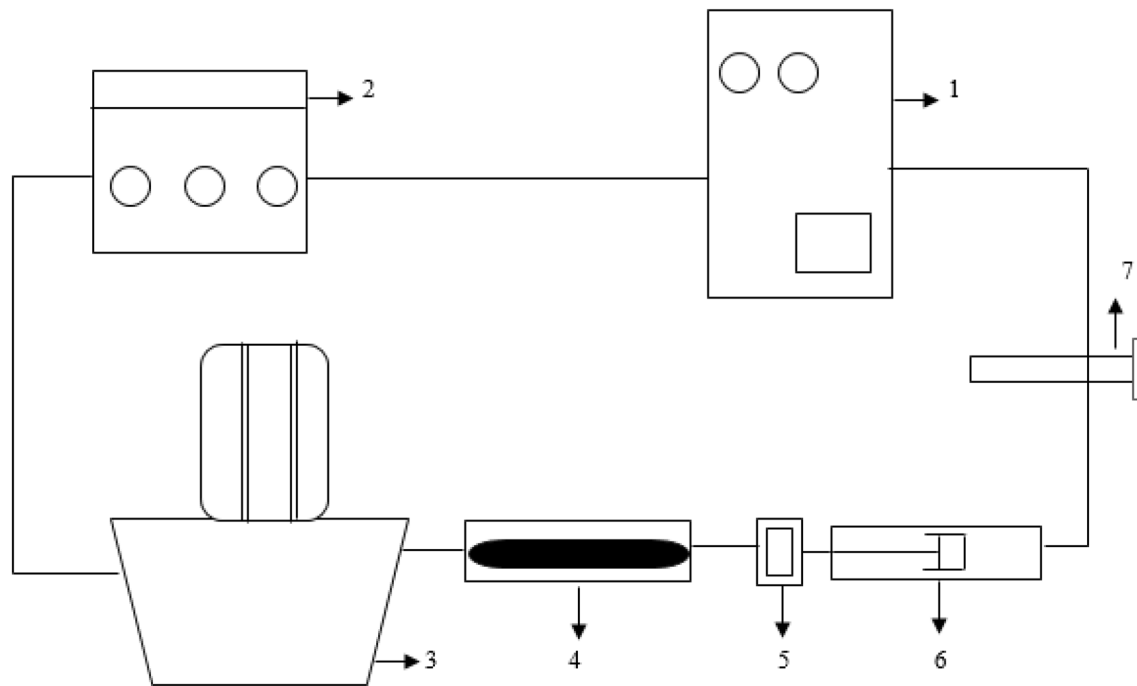


Fig. 1 Schematic representation of experimental setup. 1. Data acquisition, 2. regulated power supply, 3. hydraulic system, 4. hydraulic cylinder, 5. load cell, 6. MR damper, 7. linear variable differential transformer (LVDT)

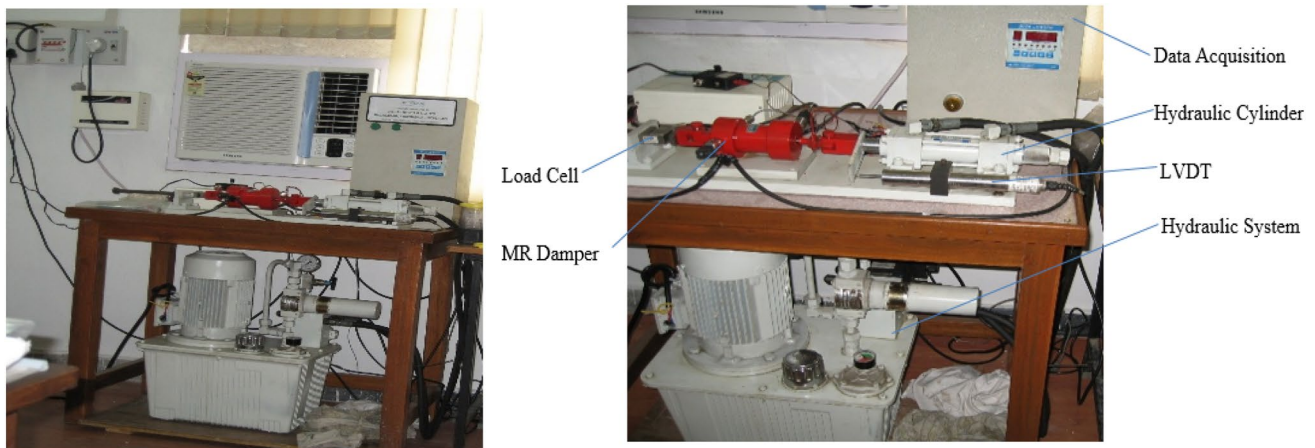


Fig. 2 Experimental set up for testing nano magnetorheological fluid damping characteristics using MR damper

with a servo hydraulic controller as displacement feedback form at a maximal speed of 20 cm/s.

Sensors and Load Cell

The displacement of damper was measured with a position sensor (Make: OPKON, Model: LPT) with a full range of 1000 mm displacement, repeatability not > 0.05% and

speed of 2 m/s. The resisting force of the damper was measured with the load cell of compression and tension kind (Make: OIML) was graded at 20 kN. The Tektronix current probe of sensitivity 100 mV/A was used to quantify the input current in the coils of MR damper. The two no. pressure transmitters (Make: SPY) having a maximum range of 200 bars was used to measure the pressure change on both sides of the damper piston.



Fig. 3 Small capacity MR damper filled with nano magnetorheological fluid

Data Acquisition

For the data attainment, a data logger (Make: Ambetronics and TC—800D model) with eight analogue units was used.

Power Supply

For testing the quasi-static damper characteristics, a LORD wonder box device controller set was used to supply the DC power of 2 amps to the coils of MR damper.

Additional Accessories

During the experiment, the damper temperature was supervised using infrared temperature probe (Make: Fluke 80T-IR) of sensitivity 1 mV/°C.

NMRF Filling Process

The fluid was de-gassed and shaken well to eliminate the microscopic air bubbles. The trapped cavities of air will consequence the force lag in the MR damper responses. To minimize the force lag and improve the damper conduct, extra care is taken while filling the fluid. The NMRF filling schematic setup is presented in Fig. 4. The following steps are followed during the filling process.

1. First, the valve 1 was locked and filled the PVC tube with NMRF.
2. To eliminate the moisture in the fluid, a vacuum pump was used for 15 min to pull the vacuum on the PVC tube.
3. Now by keeping the valve 1 closed and valve 2 opened, for 15 min, pull the vacuum on the damper housing.
4. Now by closing the valve 2 and opening the valve 1, the vacuum in the damper draws the NMRF from the PVC tube.
5. Finally, to ensure the complete fill of the damper, stroke the damper.

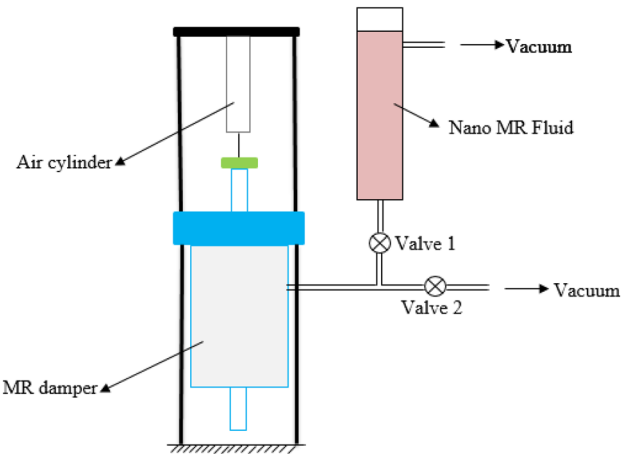


Fig. 4 Schematic representation of nano magnetorheological fluid filling set up

Dimensional and Functional Parameters of MR Damper Hydraulic Circuit

The fluid flows in the annular gap of the piston and cylinder housing when MR damper operates. The flow process is driven by certain pressure. Most of the MR dampers are operated under pressure-driven flow process (PDF). The pressure drop developed due to the PDF is approximated as summation of the viscous component (ΔP_η) and induced field-dependent yield stress component (ΔP_τ). The pressure [37] is given by

$$\Delta P = \Delta P_\eta + \Delta P_\tau = \frac{12\eta QL}{g^3 W} + \frac{C\tau_0 L}{g}, \quad (1)$$

$$Q = A_p \times V_p \quad (2)$$

$$A_p = \frac{\pi[(d_{cyl} - 2g)^2 - d_{sh}^2]}{4}, \quad (3)$$

$$c = 2.07 + \frac{12 \cdot Q \cdot \eta}{12 \cdot Q \cdot \eta + 0.4 \cdot w \cdot g^2 \cdot \tau_0}, \quad (4)$$

where L is pole length, W is width and g is gap of the flow channel. Q is volumetric flow rate, η is viscosity of fluid at zero magnetic field, τ_0 is the on state yield stress. In the present study, the proposed dimensional and functional parameters of the hydraulic circuit considered are the MR damper gap 0.0004 m, cylinder diameter 0.04 m, NMRF S and NMRF H off state viscosity (η) are 0.051 Pa.s and 0.044 Pa s, piston velocity (V_p) = 0.2 m/s, pole length (L) = 0.042 m, shear stress of the NMRF S and NMRF H samples are 1965 Pa and 948.2 Pa, width of the piston 0.1243 m, and volumetric flow rate Q is $0.2186 \times 10^{-3} \text{ m}^3/\text{s}$.

Table 2 Variation of shear stress (τ_0) and viscosity (η) of NMRF S sample with respect to current (I)

NMRF S sample		
Current (I) A	Shear stress (τ_0) Pa	Viscosity (η) Pa s
0.0	0	0.051
1.0	716.6	6.896
2.0	1286	8.232
3.0	1701	8.563
4.0	1807	8.674

Table 3 Variation of shear stress (τ_0) and viscosity (η) of NMRF H sample with respect to current (I)

NMRF H sample		
Current (I) A	Shear stress (τ_0) Pa	Viscosity (η) Pa s
0.0	0	0.044
1.0	515.3	2.291
2.0	804.8	3.051
3.0	908.9	3.712
4.0	922.7	3.907

The calculated ΔP with these parameters for NMRF S was 1339.5 kPa and for NMRF H was 914.9 kPa. Tables 2 and 3 show the variation of shear stress (τ_0) and viscosity (η) of NMRF S and NMRF H samples with respect to current (I) [38].

Results and Discussion

Force–Velocity (V_p) Behavior of NMRF

Figures 5 and 6 show the performance of the fluid that was evaluated by measuring the damping force at a prescribed triangular displacement input by varying velocities and constant input coil current. The comparison of measured data with the theoretical data is also shown. The measured damping force when no current supplied at piston velocity 0.2 m/s was 0.8 kN for NMRF S and 0.6 kN for NMRF H samples, whereas for an input current of 4.0 A and at piston velocity of 0.2 m/s, the recorded force was 1.3 kN for NMRF S and 0.9 kN for NMRF H samples. At zero current supply, the fluid in the damper exhibits viscous nature and moderate damping forces were achieved for both the samples. The viscous force exerted by the fluid is dependent on the velocity. As illustrated in Fig. 7, the damper-resisting force could be decomposed into controllable force (F_τ) due to controlled yield stress (τ_0) and uncontrollable force (F_{uc}). The uncontrollable force includes a viscous force (F_η) and a friction force (F_f). The effectiveness of the MR damper is maximized by the controllable force by maintaining a small gap:

$$F_\tau = \frac{c \cdot \tau_0 \cdot L A_p}{g} \cdot \text{sgn}(V_p) \tag{5}$$

The controlled force can be rewritten as [39]

$$F_\tau = \left(2.07 + \frac{12 \cdot Q \cdot \eta}{12 \cdot Q \cdot \eta + 0.4 \cdot w \cdot g^2 \cdot \tau_0} \right) \cdot \frac{\tau_0 \cdot L A_p}{g} \cdot \text{sgn}(V_p) \tag{6}$$

The viscous force (F_η) can be written as [39]

Fig. 5 Variation of measured and theoretical force–velocity behavior of silicone oil-based NMRF S sample in MR damper

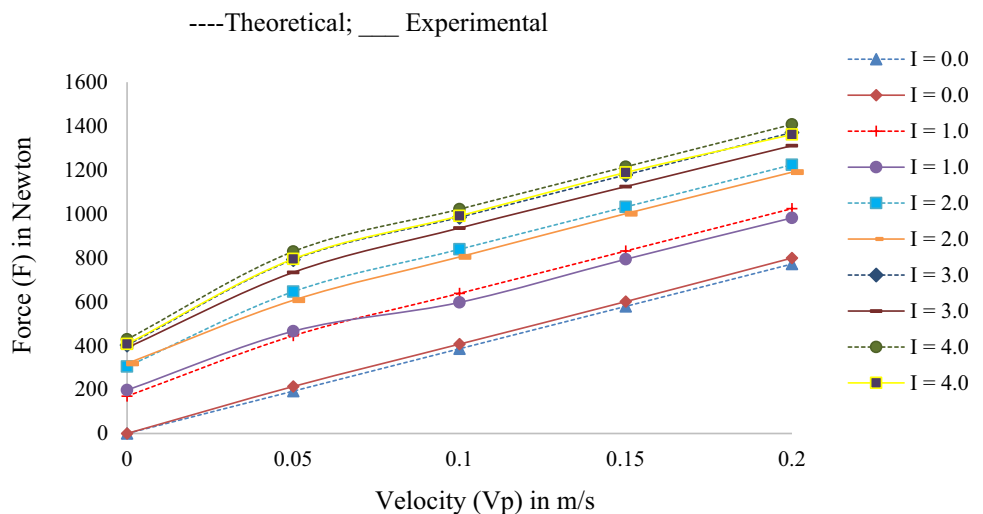


Fig. 6 Variation of measured and theoretical force–velocity behavior of hydrocarbon oil-based NMRF H sample in MR damper

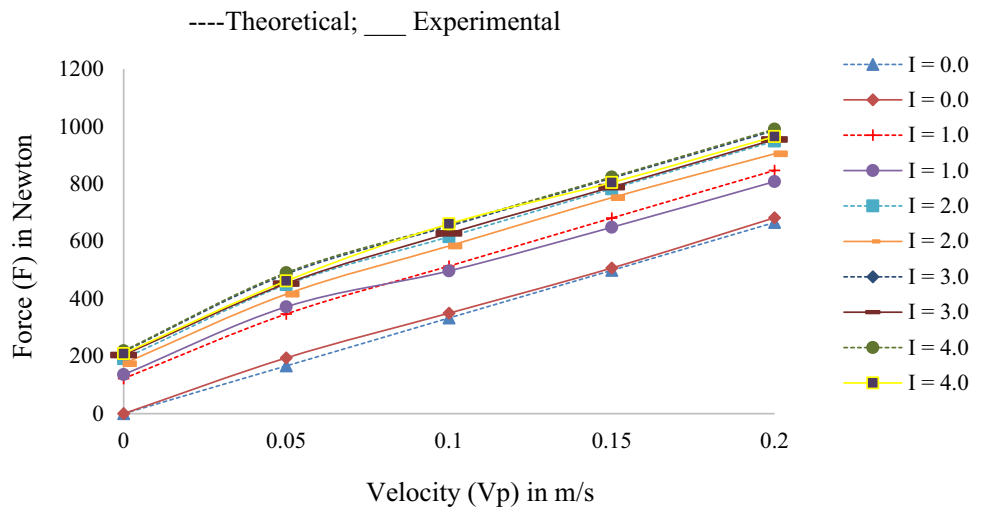
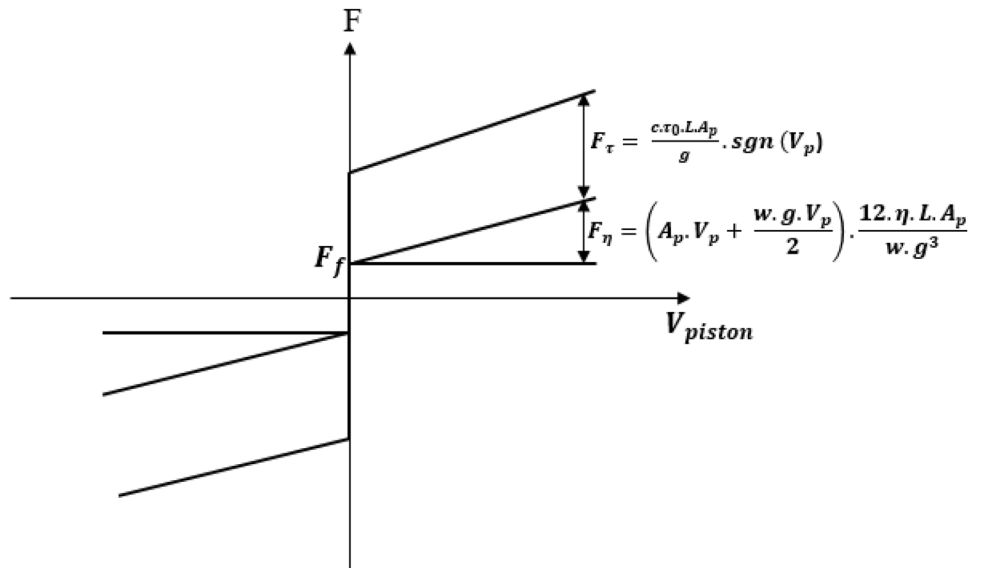


Fig. 7 Force decomposition of MR damper



$$F_{\eta} = \left(A_p \cdot V_p + \frac{w \cdot g \cdot V_p}{2} \right) \cdot \frac{12 \cdot \eta \cdot L \cdot A_p}{w \cdot g^3} \tag{7}$$

The NMRF damper’s dynamic range [40] of damper force under triangular displacement excitation for NMRF S and NMRF H sample is calculated as 1.625 and 1.5. The experiment conducted results in less dynamic range, which means the fluid samples used in MR damper are more useful in light duty applications.

The triangular waveform generated from the hydraulic actuator being linear confirms the non-interference of frictional forces and inertial forces [40] into the overall system and this permits the exact measurement of the damping force.

Force–Current (I) Behavior of NMRF

The influence of electric current on damping force under triangular displacement excitation at various constant velocity levels were measured and its comparison with the theoretical values is shown in Figs. 8 and 9 for NMRF S and NMRF H samples. It is noticed that at higher input coil current, the magnetic strength produced in the damper coil is high. Because of magnetorheology, the fluid yield stress increases, therefore, high damping forces are produced. This indicates the damping force of the fluid in MR damper depends on the strength of the applied magnetic field. The plots are parallel to each other for both the samples with less slope. The slope of the plot flattens at all the current values indicating the

Fig. 8 Variation of measured and predicted force–current (I) behavior of silicone oil-based NMRF S sample in MR damper

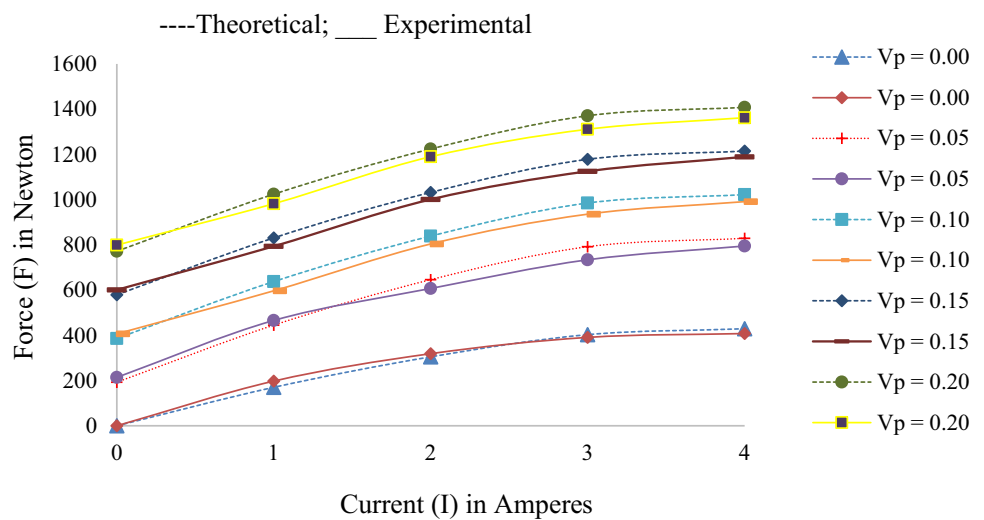
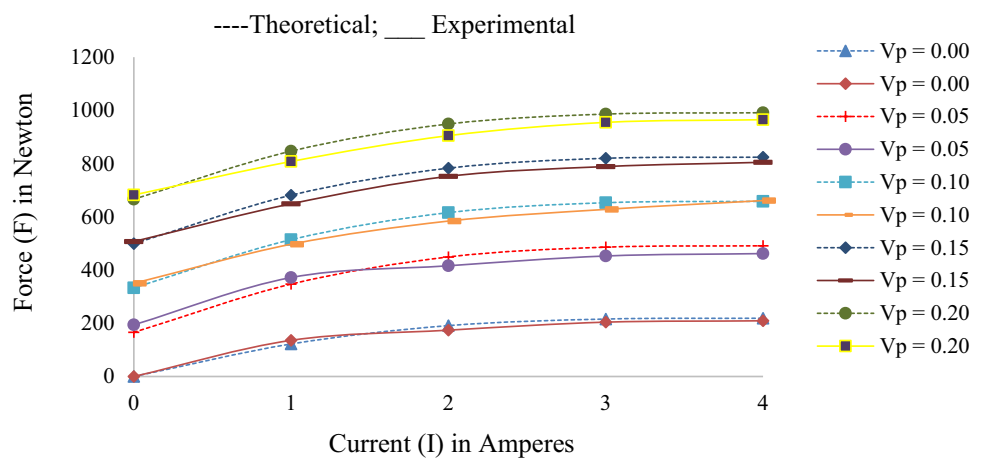


Fig. 9 Variation of measured and predicted force–current (I) behavior of hydrocarbon oil-based NMRF H sample in MR damper



dependency of damping resisting force on piston velocity (V_p) and also specifying the occurrence of damping force saturation up on reaching the current of 3.0 A for both samples. A polynomial function [41] can be used to capture this trend. The polynomial function is given as

$$A_{mr}(I) = \sum_{i=0}^n a_i I^i, \tag{8}$$

where A_{mr} is maximum damping force, I is the current supplied to the damper, ‘ a ’ is the polynomial coefficient with a suitable unit, and ‘ n ’ is the polynomial order.

Pressure–Velocity (V_p) Behavior of NMRF

The pressure velocity performance of the fluid at various constant input current levels was measured and its comparison with theoretical data for NMRF S and NMRF H samples is presented in Figs. 10 and 11, respectively. The pressure increased with the increase in velocity. When the piston moves with higher velocity, the pressure inside the

damper increases, and when the current is supplied, the NMRF transforms into a solid like paste indicating the further increase in pressure. At zero current, the linearity is due to the absence of shear stress component, whereas with increase in current and change in velocity levels, the plots of both the samples turn smooth and assembled. This indicates the influence of piston velocity on the damper pressure may be less when related to the input current of damper and also may be due to the shear thinning of the fluid at higher velocity levels.

Pressure–Current (I) Behavior of NMRF

The pressure current behavior across the annular section of the damper for NMRF S and NMRF H samples is shown in Figs. 12 and 13, respectively. The plots are not clustered and show linearity with minimal slope, this specifies the impact of piston velocity (V_p) on the damper-resisting force and pressure is considerably higher. As the input current increases, the fluid exhibits a quasi-viscous or

Fig. 10 Variation of measured and predicted pressure–velocity behavior of silicone oil-based NMRF S sample in MR damper

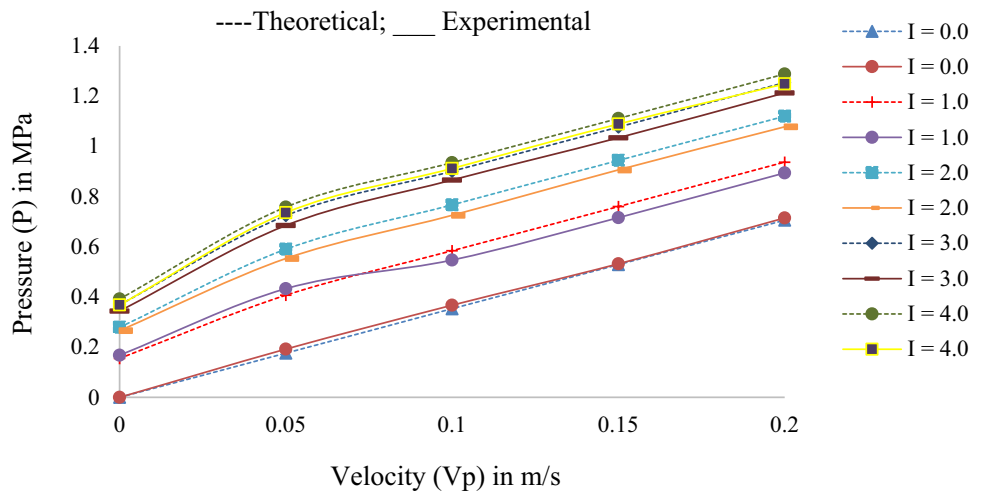


Fig. 11 Variation of measured and predicted pressure–velocity behavior of hydrocarbon oil-based NMRF H sample in MR damper

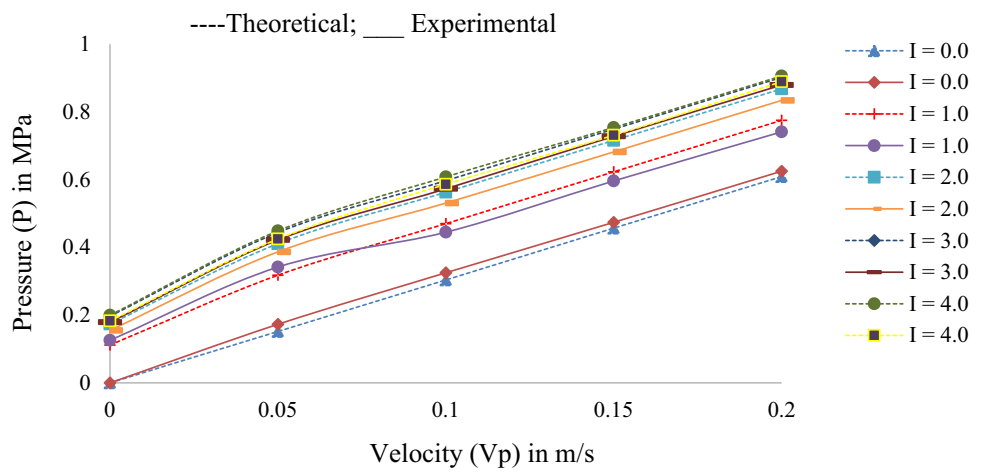
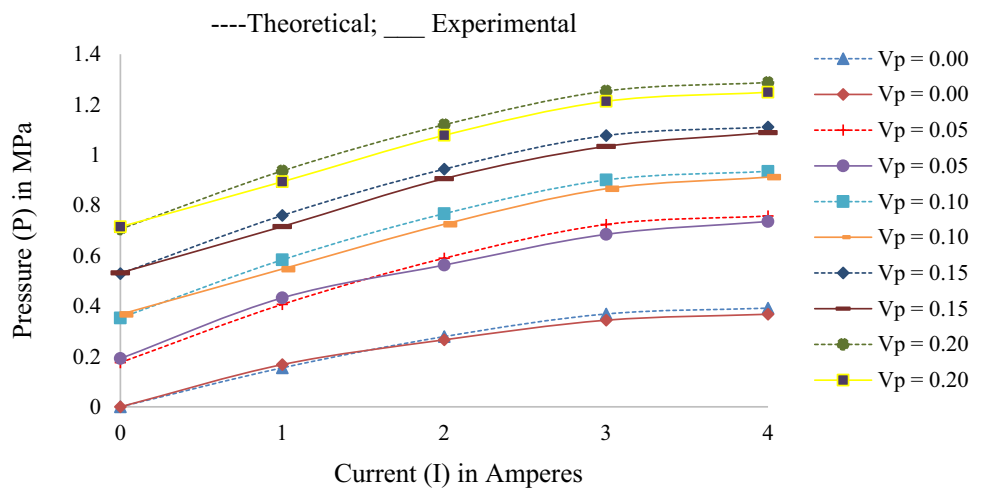


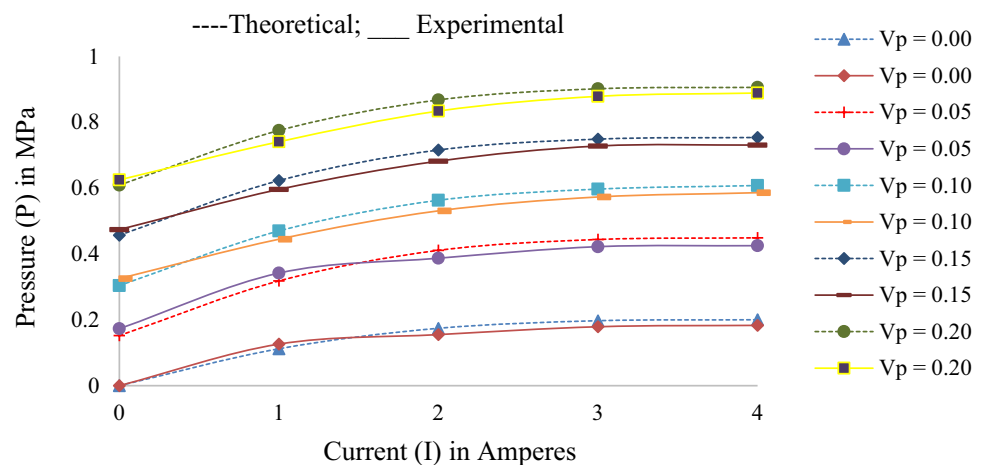
Fig. 12 Variation of measured and predicted pressure–current (I) behavior of silicone oil-based NMRF S sample in MR damper



non-Newtonian behavior. For both the samples, a crossover was observed for experimental value at piston velocity ($V_p = 0.10$ m/s), this may be because of unforeseen

frictional resistance and less efficient magnetic circuit. The measured pressure value for NMRF S sample is 1.24 Mpa and for NMRF H sample is 0.88 Mpa. When the

Fig. 13 Variation of measured and predicted pressure–current (I) behavior of hydrocarbon oil-based NMRF H sample in MR damper



piston moves, the current was induced into the fluid and the annular section of the damper was magnetized and provides the resistance to the shear flow. The increase in on state viscosity and shear yield strength of the fluid lead to formation of the chain-like aggregates [42] that opposes the fluid flow resulting in damping.

Conclusions

The quasi-static experiments were conducted to assess the performance of the nano-magnetorheological fluid (NMRF) filled in small capacity MR damper. The force–velocity (V_p), force–current (I), pressure–velocity (V_p) and pressure–current (I) behaviors were investigated at variable velocities and constant input currents under triangular displacement excitation. The fluid exhibits shear thinning effect due to this excitation. The slope for force–velocity and pressure–velocity behavior of the damper is more, whereas less slope was observed for the force–current and pressure–current conduct. The overall performance of the NMRF in MR damper is consistent without neglecting the fluid flow when the damper is subjected to excitation at lower velocity levels. The results confirm that the NMRF can be used in light-duty applications. The experimental data are in conjunction with theoretical results. The developed quasi-static model used was sufficient to define the linear behavior of the NMRF filled in MR damper under the dynamic loading for all variable tests conducted.

Declarations

Conflict of interest The authors declare that there is no conflict of interests.

References

- Nanthakumar AJD, Jancirani J (2019) Design optimization of magnetorheological damper geometry using response surface method for achieving maximum yield stress. *J Mech Sci Technol* 33:4319–4329. <https://doi.org/10.1007/s12206-019-0828-6>
- Gong X, Deng H, Yan Q, Xuan S, Ruan X (2014) Magnetorheological damper working in squeeze mode. *Adv Mech Eng* 6:1–10. <https://doi.org/10.1155/2F2014/2F410158>
- Yuan X, He H, Ling H, Tian T, Qiu T, and, (2019) A Review on structural development of magnetorheological fluid damper. *Shock Vib* 4:1–34. <https://doi.org/10.1155/2019/1498962>
- Yang G, Spencer BF Jr, Jung HJ, Carlson JD (2004) Dynamic modeling of large-scale magnetorheological damper systems for civil engineering applications. *J Eng Mech* 130:1107–1114. [https://doi.org/10.1061/\(ASCE\)0733-9399\(2004\)130:9\(1107\)](https://doi.org/10.1061/(ASCE)0733-9399(2004)130:9(1107))
- Gaddekar P, Khaire ND, Kanthale VS (2017) Magnetorheological fluid and its applications. *Int Curr Eng Technol* 7:32–37
- Bajaj H, Ugale BA, Birdi GS (2014) Application of magnetorheological (MR) fluid damper and its social impact. *Int J Mech Eng Prod Eng* 2:41–45
- Lee DY, Yamane R, Park YM, Nam Y (2009) Performance evaluation on vibration control of MR landing gear. *J Phys* 149:1–6. <https://doi.org/10.1088/1742-6596/149/1/012068>
- Luong QV, Jang D-S, Hwang J-H (2021) Semi-active control for helicopter with multiple landing gears equipped with magnetorheological damper. *Appl Sci* 11:1–18. <https://doi.org/10.3390/app11083667>
- Karunaratne NPKV (2016) Use of semi-active dampers in seismic mitigation of building structures. Thesis, Queensland University of Technology
- Bui QD, Mai D-D, Nguyen QH, Nguyen TT (2020) Development of a magnetorheological damper with self-powered ability for washing machines. *Appl Sci* 10:1–21. <https://doi.org/10.3390/app10124099>
- Valencia CH, Figueiredo KT, Vellasco M, Tanscheit R (2015) Magnetorheological damper control in a leg prosthesis mechanical. *Robot Intell Technol Appl* 3:805–815. https://doi.org/10.1007/978-3-319-16841-8_73
- Ha SH, Seong M-S, Choi S-B (2013) Design and vibration control of military vehicle suspension system using magnetorheological damper and disc spring. *Smart Mater Struct* 22:1–10. <https://doi.org/10.1088/0964-1726/22/6/065006>
- Wang J, Meng G (2001) Magnetorheological fluid devices: principles, characteristics and applications in mechanical engineering.

- Proc Inst Mech Eng 215:165–174. <https://doi.org/10.1243/2F1464420011545012>
14. Wereley NM, Cho JU, Choi SB, Choi YT (2008) Magnetorheological dampers in shear mode. *Smart Mater Struct* 17:1–11. <https://doi.org/10.1088/0964-1726/17/01/015022>
 15. Sapiński B, Goldasz J (2015) Development and performance evaluation of an MR squeeze-mode damper. *Smart Mater Struct* 24:1–14. <https://doi.org/10.1088/0964-1726/24/11/115007>
 16. Falah AH, Phule PP, Clark WW (1998) Modeling of magnetorheological fluid damper with parallel plate behavior. *Proc SPIE Smart Struct Mater* 3327:276–283. <https://doi.org/10.1117/12.310691>
 17. Zalewski R, Nachman J, Bajkowski J, Shillor M (2014) Dynamic model for a magnetorheological damper. *Appl Math Model* 36:2366–2376. <https://doi.org/10.1016/j.apm.2013.10.050>
 18. Guo S, Pan C, Yang S (2006) Dynamic Modelling of magnetorheological damper behaviors. *Mater Syst Struct* 17:3–14. <https://doi.org/10.1177/1045389X06055860>
 19. Bajkowski J, Nachman J, Shillor M, Sofonea M (2008) A model for a magnetorheological damper. *Math Comput Model* 48:56–68. <https://doi.org/10.1016/j.mcm.2007.08.014>
 20. Kubik M, Goldasz J (2019) Multiphysics model of an MR damper including Magnetic hysteresis. *Shock Vib* 3:1–20. <https://doi.org/10.1155/2019/3246915>
 21. Yu J, Xiaomin D, Zhang Z (2017) A novel model of magnetorheological damper with hysteresis division. *Smart Mater Struct* 26:1–15. <https://doi.org/10.1088/1361-665X/aa87d6>
 22. Spencer BF, Carlson JD, Sain MK, Dyke SJ (1997) Phenomenological model for magnetorheological dampers. *J Eng Mech* 123:230–238. [https://doi.org/10.1061/\(ASCE\)0733-9399\(1997\)123:3\(230\)](https://doi.org/10.1061/(ASCE)0733-9399(1997)123:3(230))
 23. Huang L, Li J, Zhua W (2017) Mathematical model of a novel small magnetorheological damper by using outer magnetic field. *AIP Adv* 7:035114–035212. <https://doi.org/10.1063/1.4978866>
 24. Yao GZ, Yap FF, Chen G, Li WH, Yeo SH (2002) MR damper and its application for semi-active control of vehicle suspension system. *Mechatronics* 12:963–973. [https://doi.org/10.1016/S0957-4158\(01\)00032-0](https://doi.org/10.1016/S0957-4158(01)00032-0)
 25. Pavic G (2018) Analysis of vibration reduction by damping using simple analytical modelling. *Shock Vib*. <https://doi.org/10.1155/2018/1098531>
 26. Gordaninejad F, Hansen BC, Ericksen EO, Chang F-K, Saiidi S (2002) Magneto-Rheological fluid dampers for control of bridges. *J Intell Mater Struct* 13:167–180. <https://doi.org/10.1177/104538902761402567>
 27. Chen ZH, Lam KH, Ni YQ (2016) Enhanced damping for bridge cables using a self-sensing MR damper. *Smart Mater Struct* 25:1–13. <https://doi.org/10.1088/0964-1726/25/8/085019>
 28. Kim B-G, Kang BH, Han C, Choi SB (2018) Design and analysis of a Magnetorheological damper for aircraft landing gear. *Active and passive smart integrated struct*. *Proc SPIE*. <https://doi.org/10.1117/12.2296757>
 29. Aly AM (2013) Vibration control of buildings using magnetorheological damper: a new control algorithm. *J Eng* 9:1–11. <https://doi.org/10.1155/2013/596078>
 30. Shrimali MK, Bharti SD, Dumne SM (2015) Seismic response analysis of coupled building involving MR damper and elastomeric base isolation. *Ain Shams Eng J* 6:457–470. <https://doi.org/10.1016/j.asej.2014.12.007>
 31. Bui QD, Nguyen HQ, Hoang VL, Mai DD (2021) A new self-adaptive magnetorheological damper for washing machines. *Smart Mater Struct* 30:1–12. <https://doi.org/10.1088/1361-665X/abcd09>
 32. Ulasyar A, Lazoglu I (2018) Design and analysis of a new magnetorheological damper for washing machine. *J Mech Sci Technol* 32:1549–1561. <https://doi.org/10.1007/s12206-018-0308-4>
 33. Guan XC, Ou JP, Guo PF (2011) Modeling and analyzing of hysteresis behaviour of magnetorheological dampers. *Procedia Engg* 14:2756–2764. <https://doi.org/10.1016/j.proeng.2011.07.347>
 34. Cortes-Ramirez JA, Viilarreal-Gonzfilez LS, Martinez-Martinez M (2007) Characterization, modeling and simulation of magnetorheological damper behavior under triangular excitation. In: *Mechatronics for safety, security and dependability in a new era* 1:353-358. <https://doi.org/10.1016/B978-008044963-0/50072-2>
 35. Khan SA, Suresh A, Seetharamaiah N (2014) Principles, characteristics and application of magnetorheological fluid damper in flow and shear mode. *Procedia Mater Sci* 6:1547–1556. <https://doi.org/10.1016/j.mspro.2014.07.136>
 36. Yagnasri P, Seetharamaiah N, Usha Sri P (2022) Synthesis and rheological characterization of nano magnetorheological fluid using inverse spinel ferrite (NiFe₂O₄). *Int J Appl Ceram Technol*. <https://doi.org/10.1111/ijac.14031>
 37. Sailaja G, Seetharamaiah N, Janardhana M (2016) Design and finite element analysis of MR fluid damper for structural vibration mitigation. *Int J Mech Eng Technol* 7:143–151. <http://www.iaeme.com/ijmet/issues.asp?JType=IJMET&VType=7&IType=4>
 38. Yagnasri P, Seetharamaiah N, Usha Sri P (2021) Magnetorheological performance of nano magnetorheological (MR) fluid based on NiFe₂O₄ nanoparticles. *Nano World J* 7(1):1–7. <https://doi.org/10.17756/nwj.2021-085>
 39. Zhao-DongXu Y-Q, Jun-TaoZhu F-H (2017) Design and parameters optimization on intelligent control devices. *Intell Vib Control Civ Eng Struct*. <https://doi.org/10.1016/B978-0-12-405874-3.00005-9>
 40. Feng ZY, Hua-ling C (2006) Study on damping properties of magnetorheological damper. *Front Mech Eng* 4:452–455. <https://doi.org/10.1007/s11465-006-0057-4>
 41. Song X, Ahmadian M, Southward SC (2005) Modeling magnetorheological dampers with application of nonparametric approach. *J Intel Mater Syst Struct* 16:421–432. <https://doi.org/10.1177/2F1045389X05051071>
 42. Li DD, Yeoh GH, Lam H-F, Timchenko V (2017) Numerical modeling of magnetic nanoparticle and carrier fluid interactions under static and double shear flows. *IEEE Trans Nanotechnol* 16:798–805. <https://doi.org/10.1109/TNANO.2017.2691018>

Publisher's Note Springer Nature remains neutral with regard to jurisdictional claims in published maps and institutional affiliations.